Ionization of ethane, butane, and octane in strong laser fields

Sasi Palaniyappan, Rob Mitchell, N. Ekanayake, A. M. Watts, S. L. White, Rob Sauer, L. E. Howard, M. Videtto, C. Mancuso, S. J. Wells, T. Stanev, B. L. Wen, M. F. Decamp, and B. C. Walker
Physics and Astronomy Department, University of Delaware, Newark, Delaware 19716, USA
(Received 8 December 2009; revised manuscript received 10 September 2010; published 26 October 2010)

Strong-field photoionization of ethane, butane, and octane are reported at intensities from 10^{14} to 10^{17} W/cm^2. The molecular fragment ions, C^+ and C^{2+}, are created in an intensity window from 10^{14} to 10^{15} W/cm^2 and have intensity-dependent yields similar to the molecular fragments $C_mH_n^+$ and $C_mH_n^{2+}$. In the case of C^+, the yield is independent of the molecular parent chain length. The ionization of more tightly bound valence electrons in carbon (C^{3+} and C^{4+}) has at least two contributing mechanisms, one influenced by the parent molecule size and one resulting from the tunneling ionization of the carbon ion.

DOI: 10.1103/PhysRevA.82.043433 PACS number(s): 32.80.Fb, 32.80.Rm, 33.80.Rv, 33.20.Xx

I. INTRODUCTION

The interaction of molecules with intense pulsed laser light has been an active research area for decades. Molecules in strong fields exhibit effects such as field alignment [1–3], laser control of the molecular orientation [4–6], stabilization [7], enhanced ionization [8–11], dissociation, and Coulomb explosion [12–14]. Much of the earlier research in laser-molecule interactions studied dynamics such as ionization and fragmentation using mass and momentum spectroscopy. There has been a long-standing interest in the high-charge-state ion production from hydrocarbon molecules in strong fields [15–18]. When a molecule interacts with a strong laser field ($>10^{13}$ W/cm^2), one or more valance electrons can be stripped away from the parent molecule through molecular field ionization [19], an analog of the well-known tunneling ionization in atoms [20]. This has been shown to be especially true for σ-bond systems such as CH_3-Br [21], CH_3-X, linear alcohols, and alkanes [22–25], which respond in an "atomic-like" fashion for the removal of the first electron by tunneling. In general however, molecular ionization is more complicated than atomic ionization with charge resonant excitation and enhanced ionization pathways [26] due to the extended Coulomb potential in the molecular structure. For example, with enhanced ionization in molecules, the combination of superposed Coulomb potentials and the applied laser electric field leads to a critical bond distance at which tunneling ionization is increased due to the reduction in the effective potential between the nuclei [27]. This mechanism helped explain observations of fragment ion kinetic energies [28], which are significantly lower than the values expected for prompt ionization and Coulomb explosion at the equilibrium bond length. Nonadiabatic excitation is also possible in molecules and the dependence of ionization on molecular size has been an area of ongoing research [26,29].

Recent experiments have focused on electron ionization dynamics during the laser-molecule interaction. For example, during ionization the photoelectron may recollide with the parent ion when it is driven back by the laser field as it reverses on the next half cycle. Electron-ion recollision leads to nonsequential ionization (NSI) [30], high-order-harmonic generation (HHG) [31], and the much reported probing of molecular dynamics with attosecond resolution pulses [32,33].

In the new frontier of ultrastrong-field laser science (up to 10^{20} W/cm^2), one naturally expects molecules will ionize to higher charge states. At this time though, it is not known how this will occur and what role will be played by strong-field mechanisms such as enhanced ionization or Coulomb explosion. Results on laser fusion with methane clusters highlight the potential of strong and ultrastrong-field interactions with hydrocarbon systems [34–36]. It was recently reported in an ultrastrong-field ionization study of methane that C^{n+} ($n \leqslant 5$) atomic fragmental ions are created through processes that develop from a nonadiabatic or molecular response (C^{2+} and C^{3+}, at intensities from 10^{14} to 10^{15} W/cm^2) to an adiabatic or atomic-like response (C^{5+}, at intensities from 10^{15} to 10^{19} W/cm^2) [37]. It is unclear whether this response of methane to a strong or ultrastrong laser field can be generalized to other molecules or whether different mechanisms are involved for larger or nonsymmetric molecules. In this paper, we begin to address this question by measuring the fragmentation and intensity-dependent ion yields from the linear chain hydrocarbons ethane, butane, and octane.

II. EXPERIMENTAL SETUP

The experimental apparatus consisted of a kilohertz Ti:sapphire laser (3 mJ, 790 nm, 45 fs), terawatt Ti:sapphire laser (80 mJ, 35 fs, 790 nm) [38,39], and a high-resolution, time-of-flight ion spectrometer with ion gating to prevent detector saturation (Fig. 1). The high intensity was created by focusing the laser with a gold-coated, f/2 off-axis parabolic mirror in an ultrahigh vacuum chamber. A skimmed, 0.5-mm wide effusive molecular beam was crossed with the laser focus.

A linearly polarized laser electric was used in these studies with orientations perpendicular and parallel to the time-of-flight axis. The field extraction plates before the time-of-flight region used 1 mm apertures for resolving the fragmentation emission angle (5° resolution) and 15 mm apertures with 3 kV/cm extraction fields for collecting the total integrated yield. Collecting the fragments in these configurations ensured accurate ion collection regardless of the fragment momentum distribution and eliminated the possibility of skewed results due to aperturing of ion trajectories in the mass spectrometer. The anisotropy in the angular distribution for the C^{n+}

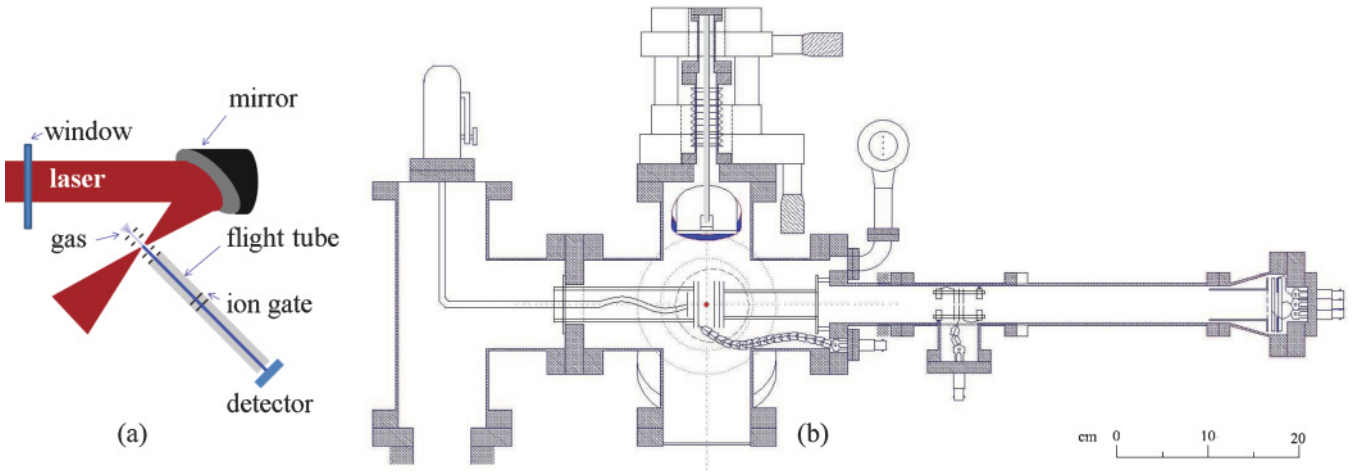

FIG. 1. (Color online) (a) Experimental setup showing the 45 focusing parabolic mirror (in a vacuum) with the gas jet and time-of-flight spectrometer. (b) A scale drawing of the spectrometer showing the gas source on the left, interaction chamber in the center, and the time-of-flight region on the right. The parabolic mirror assembly is in the top center section of (b).

fragments (i.e., C^{n+} yield parallel to E divided by C^{n+} perpendicular to E) varied across the molecular species being the greatest for ethane and the smallest for methane. The characterization of the momentum distributions [40,41] will certainly be the subject of future study. The intensity-dependent ion yield data for C^{n+} presented in the figures is summed over all momentum and the results represent the net yield.

To eliminate degeneracy in the mass spectrum (e.g., $^{12}C^{4+}$:$^{12}CH_3^{5+}$) we verified the ^{12}C collections with ^{13}C. In the case of ethane both the ^{12}C atoms were replaced by ^{13}C and for butane the terminal ^{12}C atom was replaced by ^{13}C. The data are averaged into 10% intensity bins and each data point represents typically three independent collections of 10^5 shots. Ionization saturated in the collections at approximately 10^5 ions/shot torr. The laser intensity is calibrated to within 50% by measuring the ion yields of krypton [42]. The ion and electron signal error is estimated to be a factor of 3.

III. EXPERIMENTAL RESULTS

A. Ethane fragmentation

Figures 2(a) through (c) show the observed ions from ethane at intensities of 4.5×10^{14}, 1.5×10^{14} , and 5×10^{13} W/cm^2 as a function of the ion "m/q" ratio, where "m" and "q" are the ion mass and charge, respectively. Figure 2(a) displays the molecular parent ion $C_2H_6^+$, singly charged molecular fragmental ions ($C_2H_5^+$ to C_2H^+), a variety of molecular fragmental ions (for example, C_2H^+, $C_2H_5^{2+}$), and atomic fragmental ions C^+ and C^{2+}. The most abundant species are $C_2H_n^+$ followed by the CH_n^+ peaks and finally $C_2H_n^{2+}$, which is approximately 10% of CH_n^+ and comparable to the C^+ and C^{2+} yield.

The asterisks in Figs. 2(b) and 2(c) on the peaks in the ion spectrum mark the corresponding peak of the same ion on Fig. 2(a) scaled down by a constant factor (i.e., the ratio of the $C_2H_6^+$ parent ion count at the different intensities). These are added to the figure to elucidate the differences in the intensity dependence between the molecular ion $C_2H_6^+$ and the observed molecular fragmental ions. As one can see in the figure, the ion peak asterisk envelope in Fig. 2(a) matches well to the corresponding ion peaks in Fig. 2(b) considering the typical nonlinearity of the strong-field processes and the factor of 3 change in the intensity between the collections. Whether due to a lower branching ratio or a slightly different intensity dependence, as the intensity drops by another factor of 3 from 1.5×10^{14} to 5×10^{13} W/cm^2, lower m/q fragments drop below our detection limit. Overall though, the proportionate decrease of the fragment yields over such a large change in intensity requires a nearly identical production rate for the parent ion and molecular fragments. In addition, the final product m/q ion distributions in our study are similar to those observed by electron impact dissociative ionization [43]. From

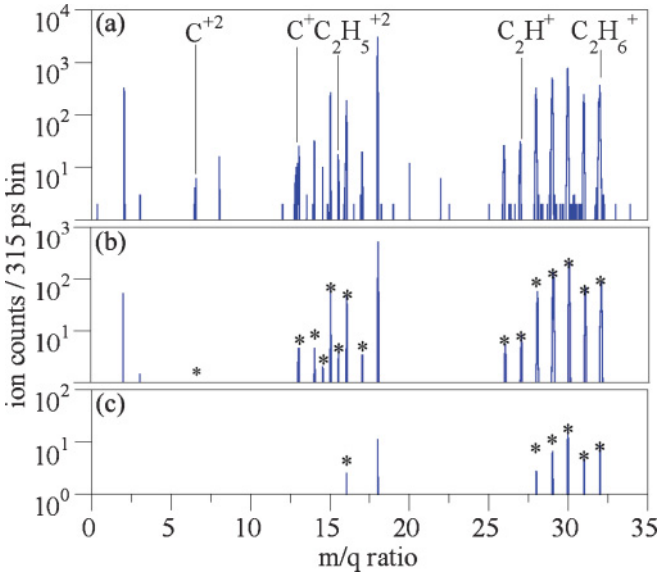

FIG. 2. (Color online) Measured time-of-flight ion spectra from ethane at an intensity of (a) 4.5×10^{14} W/cm^2, (b) 1.5×10^{14} W/cm^2, and (c) 5×10^{13} W/cm^2. Only a few of the observed ion peaks are labeled here. The asterisk marks on (b) and (c) represent the corresponding peaks in (a). The peak at $m/q = 18$ is water from the background.

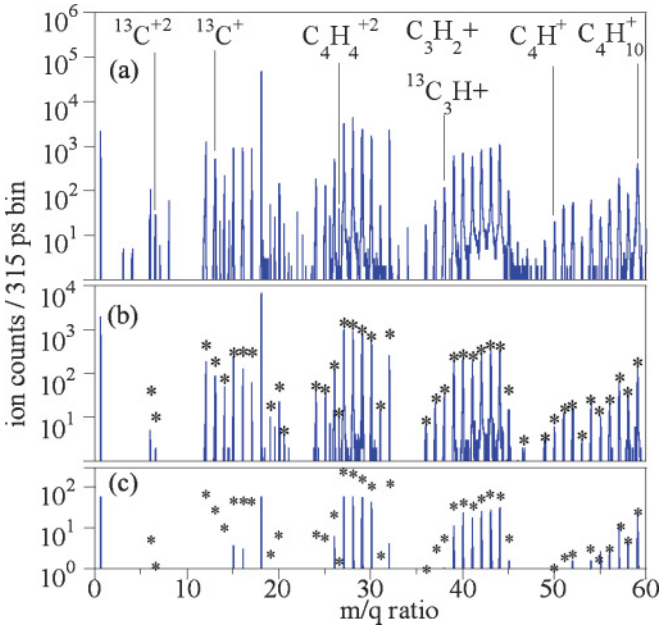

FIG. 3. (Color online) Measured time-of-flight ion spectra from butane at an intensity of (a) 1.4×10^{15} W/cm^2, (b) 4.5×10^{14} W/cm^2, and (c) 1.5×10^{14} W/cm^2. Only a few of the observed ion peaks are labeled here. The asterisk marks on (b) and (c) represent the corresponding peaks in (a). The peak at $m/q = 18$ is water from the background.

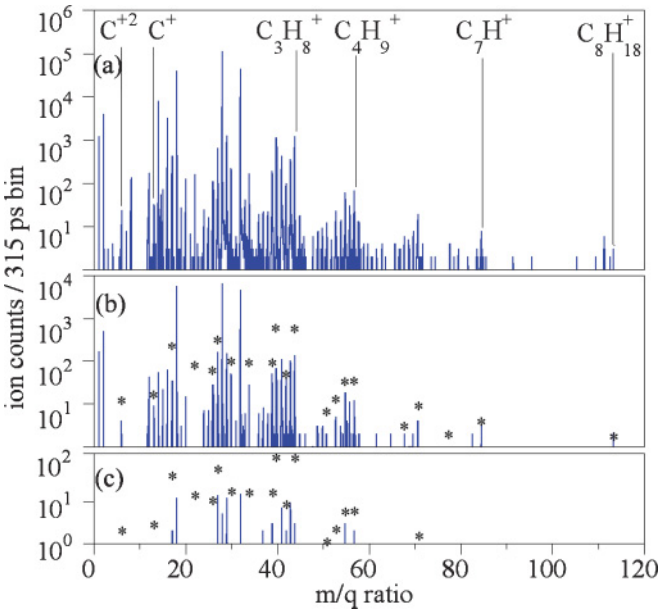

FIG. 4. (Color online) Measured time-of-flight ion spectra from octane at an intensity of (a) 4.5×10^{14} W/cm^2, (b) 1.5×10^{14} W/cm^2, and (c) 5×10^{13} W/cm^2. Only a few of the observed ion peaks are labeled here. The asterisk marks on (b) and (c) represent the corresponding peaks in (a). The peak at $m/q = 18$ is water from the background.

5×10^{13} to 4.5×10^{14} W/cm^2 the similarity in the intensity dependence of the yields we observe is consistent with the previously observed molecular excitation via nonadiabatic excitation [44] as well as the creation of a superexcited state [45] which decays into the final neutral and charged fragments.

B. Butane fragmentation

Figures 3(a) through (c) display the ions from butane at intensities of 1.4×10^{15}, 4.5×10^{14}, and 1.5×10^{14} W/cm^2 as a function of the ion "m/q" ratio. The figure shows the molecular parent ion $C_4H_{10}^+$, a variety of molecular fragmental ions ($C_4H_{10}^+$, C_4 H^+, $^{13}C_3H^+$, $C_3H_2^+$, and $C_4H_4^{2+}$), and atomic fragmental ions C^+ and C^{2+}. One should note the potential degeneracy in molecular fragmental ions (e.g., $^{13}C_3H^+$:$C_3H_2^+$ or C_2 H_2^{2+}:CH^+). The most abundant fragments are $C_2H_n^+$ near $m/q \approx 30$, which is the same as for ethane despite the factor of 2 change in the parent ion size. Double-charged fragments (e.g., $C_4H_4^{2+}$) are a few percent of the abundance of the prominent $C_2H_n^+$ fragments. Comparing the fragmentation pattern to that observed by the collisional excitation of butane [46], there is an overall similarity in the relative abundance of $C_4H_n^+$, $C_3H_n^+$, $C_2H_n^+$, and CH_n^+ despite the differences in the excitation and ionization of the molecule by the laser field or electron collision.

As in the case of ethane, we see the asterisk-marked peak envelope in Fig. 3(a) matches the corresponding peaks in Figs. 3(b) and 3(c) with few exceptions from the parent ion ($m/q = 59$) to C^+ ($m/q = 13$) and indicates a nearly identical intensity-dependent production rate for these species. Lower m/q values are less abundant and drop from our detection limit in Fig. 3(c) as the intensity is decreased to 1.5×10^{14} W/cm^2. From Fig. 3, the intensity-dependent fragmentation branching can be seen to be very robust from the parent ion $m/q = 59$ values one-half of the parent $m/q \approx 30$ over a decade in intensity from 1.5×10^{14} to 1.4×10^{15} W/cm^2.

C. Octane fragmentation

Figures 4(a) through (c) show the ions from octane at intensities of 4.5×10^{14}, 1.5×10^{14}, and 5×10^{13} W/cm^2. We observe the molecular parent ion $C_8H_{18}^+$, a variety of molecular fragmental ions (for example, C_7H^+, $C_4H_9^+$, $C_3H_8^+$), and atomic fragmental ions C^+ and C^{2+}. Due to the unavailability of octane with a ^{13}C isotope, we used only a ^{12}C octane. The most abundant ion is again the $m/q \approx 30$ $C_2H_n^+$, followed by CH_n^+ and $C_3H_n^+$ roughly equal in their yield, but lower by a factor of approximately 3 than $C_2H_n^+$. Other fragments (e.g., $C_4H_n^+$) are 10% or less than the yield of $C_2H_n^+$.

Here also we see the asterisk envelope in Fig. 4(a) matches the corresponding peaks in Figs. 4(b) and 4(c) from the parent ion to C^+ with few exceptions. At 5×10^{13} W/cm^2 the general branching pattern at $m/q = 30$, 40, and 55 (i.e., $C_2H_n^+$, $C_3H_n^+$, and $C_4H_n^+$, respectively) can be identified, however, fewer fragments with less variation in their hydrogenation makes the spectrum visibly different at the lower intensity.

D. Ionization yields of carbon fragments

Figure 5(a) shows the measured atomic fragmental ions C^{n+} ($n \leqslant 4$) from ethane at intensities from 4×10^{13} to 1×10^{17} W/cm^2. Also shown in the figure are calculated ionization yields, which will be discussed later. The measured

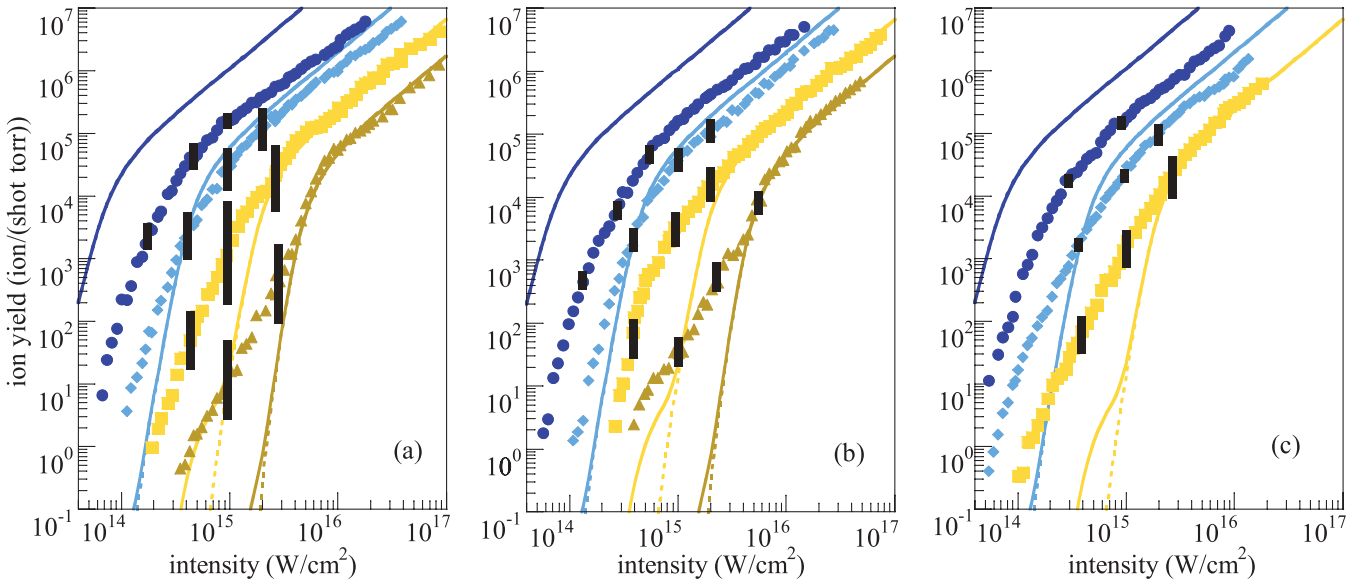

FIG. 5. (Color online) C^{1+} (dark blue circles), C^{2+} (light blue diamonds), C^{3+} (yellow squares), and C^{4+}(gold triangles) fragments from (a) ethane, (b) butane, and (c) octane with calculated ADK (dashed lines) and total yields (solid lines). The bars indicate the momentum anisotropy for C^{n+} fragments at that intensity. The smallest bars for C^+ (which has an anisotropy ratio between 1 and 1.6) are barely visible within the data.

ionization yields for C^+ and C^{2+} increase smoothly with an I^5 dependence from the detection threshold of 1 ion/shot torr to saturation at 10^5 ions/shot torr. Above 10^5 ions/shot torr the yield is saturated and the intensity dependence of the yield is $I^{3/2}$ as expected for collections from a Gaussian laser focus. The observed intensity dependence for C^+ and C^{2+} is also close to that observed for the molecular fragments in Fig. 2 with an appearance near 5×10^{13} W/cm^2 and saturation near 3×10^{14} W/cm^2. The yields of C^{3+} and C^{4+} are more complicated. Most apparent is the presence of a characteristic "knee" structure in the intensity-dependent ion yield at a few percent of the saturated yield (i.e., 10^2 ions/shot torr to 10^3 ions/shot torr). In both atomic and molecular studies, this knee is often associated with NSI due to recollision in the strong-field laser-atom interaction [47,48].

Figure 5(b) shows the measured atomic fragmental ions C^{n+} ($n \leqslant 4$) from butane at intensities from 4×10^{13} to 1×10^{17}W/cm^2 along with the calculated yields. Looking at Fig. 5, one realizes the measured ion yields of C^{n+} from butane look very similar to those of ethane. Within experimental uncertainties, the measured C^+ and C^{2+} yields for ethane and butane are, in fact, indiscernible. For C^{3+} and C^{4+}, the saturation intensity (yield near 10^5 ions/shot torr) is the same when compared between butane and ethane; however, the yields in the knee region (10^2 ions/shot torr to 10^3 ions/shot torr) are different between the two species with a slightly higher ionization yield in butane when compared to ethane at the same intensity. For C^{3+}, the knee structure is not clear since the knee and sequential ionization yields are comparable and not clearly separable as is the case when NSI charge states saturate at very different intensities and the NSI yield is a percent or less of the sequential yield [48].

Having measured the C^{n+} ion yields from ethane and butane, we then want to measure the same from octane. Figure 5(c) shows the measured atomic fragmental ions C^{n+} ($n \leqslant 3$) from octane at intensities from 4×10^{13} to 3×10^{16} W/cm^2 along with the corresponding calculated ion yields expected for atomic carbon. Due to the degeneracy (e.g., C^{4+}:CH_3^{5+}) and the lack of ^{13}C isotope octane, it was not possible to measure the C^{4+} ion yield from octane. As one can see in the figure, the results for C^+ in octane are the same as those of ethane and butane. C^{2+} and C^{3+} show identical saturation intensities across the species, but the knee ionization yield in the signal range 10^2 ions/shot torr to 10^3 ions/shot torr observed in C^{3+} and C^{4+} for butane now involves lower charge states; an enhancement in the yield below 10^3 ions/shot torr at 10^{14} W/cm^2 is evident for C^{2+} with octane.

As additional information, the momentum anisotropy (i.e., theratio of the parallel to perpendicular yield) is shown across the collection intensities in the total ion yields. This ratio is represented by bars amidst the data of Figs. 5(a), 5(b), and 5(c). The length of the bar gives the ratio of the parallel and perpendicular yield at that intensity. For example, in Fig. 5(b) the 3.4×10^3 ions/shot torr C^{3+} yield from butane at 1×10^{15} W/cm^2 varies by a factor of 2.4 between the parallel and perpendicular components. The bar representing that anisotropy ranges from the minimum value of 2.2 10^3 ions/(shot torr) for the perpendicular yield to 5.2×10^3 ions/(shot torr) for the yield parallel to the electric field.

Finally, we want to carefully compare the experimental C^+ and C^{4+} ion yields from methane [37], ethane, butane, and octane. Figure 6 shows the measured C^{n+} ion yields from methane ($n = 4$), ethane ($n = 1,4$), butane ($n = 1,4$), and octane ($n = 1$) from a linearly polarized field at intensities from 3×10^{13} to 1×10^{17} W/cm^2. As seen in the figure, the C^+ ion yields from ethane, butane, and octane are indistinguishable within experimental error. Recalling from previous figures, at saturation the C^{4+} ion yields from methane, ethane,

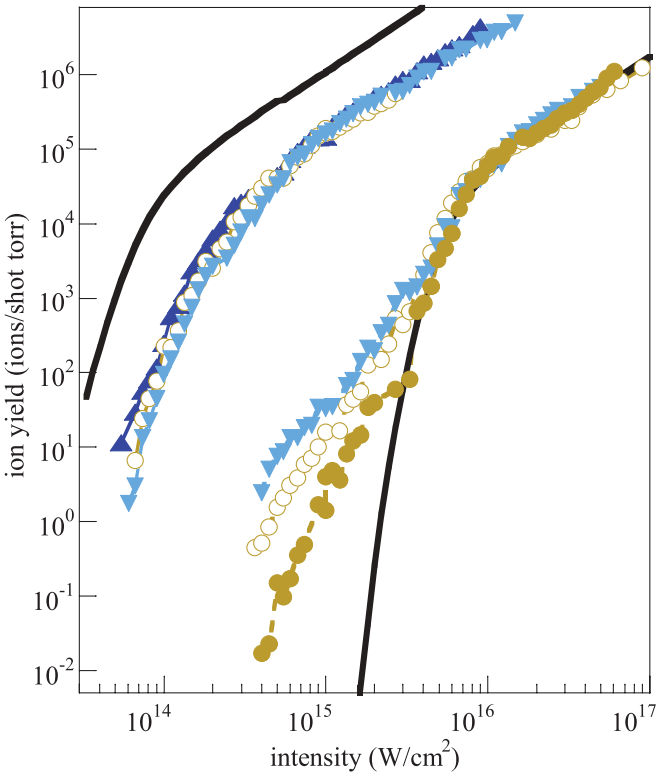

FIG. 6. (Color online) C^+ and C^{4+} fragments from methane (solid yellow circles) (C^+ from methane not shown), ethane (open yellow circles), butane (light blue inverted triangles), and octane (dark blue triangles) (C^{4+} from octane not shown) with lines shown between the data points to aid the eye. The calculated ADK, C^+, and C^{4+} tunneling ionization yield is also shown (thick black line).

and butane are also identical. Below saturation, however, a clear trending in the ion yields can be observed as one moves from smaller to larger molecules. This is most evident in the knee region of C^{4+} where the rate responsible for this component in the yield can be seen to increase in the intensity range of 10^{15} W/cm^2 (ion yield of ~10 ions/shot torr) with the size of the parent molecule. At an intensity of 1×10^{15} W/cm^2, the C^{4+} ion yield from ethane and butane are a factor of 4 and 10 higher than that of methane, respectively. Not shown in the figure is the similar, though less prominent, increase also present in the lower intensity regions of the C^{2+} and C^{3+} yields where the ion yields in the count region 10 ions/shot torr to 1000 ions/shot torr are enhanced with a larger molecular parent ion size. The calculated atomic ionization yields (described in the next section) are also shown in Fig. 6.

IV. THEORY

To better understand the ionization, we have used a three-dimensional (3D), relativistic, semiclassical, single-electron model of ionization described previously [42]. Briefly, the model is a three-step process comprised of (1) tunneling ionization followed by (2) continuum photoelectron dynamics and then (3) recollision interactions between the continuum photoelectron and the parent ion incorporating $(e,2e)$ and $(e,3e)$ scattering cross sections. With the laser and focus parameters from the experiment [800 nm center wavelength, f/2 TEM_{00} focus, and 40 fs full width at half maximun (FWHM) Gaussian temporal profile] the model calculates field ionization using the tunneling rate of Ammosov, Delone, and Krainov (ADK) [20]. We approximate the carbon within the alkanes as free atoms. Starting at the neutral carbon atom, the ionization is evaluated sequentially with increasing charge. The rate equations are solved in time for each atom or ion across the laser focus. This method best represents the ionization within the laser focus from multiple charge states.

Following ionization, we use classical trajectory ensembles to simulate the tunneling photoionization current and continuum dynamics. Photoelectron dynamics are calculated by solving the relativistic equations of motion using a Runge-Kutta ordinary differential equation solver with a relative error tolerance threshold of 10^{-6}, local error threshold of 10^{-12}, and ~0.015 fs time step. Including or omitting the Coulomb field of the core ion did not significantly affect the final yields. The calculation is considered in the low-density limit so space-charge effects are not included.

The impact ionization cross sections, when multiplied by the recollision flux from the photoionization current, give our calculated (e,ne) nonsequential ionization due to recollision interactions. $(e,2e)$ and $(e,3e)$ cross sections were obtained from the experiments [49] and the Born-Bethe scaling law [42]. Excitation cross sections [49] were included for C^{3+} and C^{4+} assuming they lead to prompt ionization. We note while (e,ne) cross sections for many of the chain hydrocarbon ions have not been measured, the cross section for neutral methane to form C^+ is ~20% of the C to C^+ cross section [50]. Since the molecular bond influence on carbon is minimized for tightly bound electrons, the atomic recollision approximation is expected to be most valid for C^{4+} with impact energies above 100 eV.

The calculated yields are shown in Figs. 5 and 6 with the sequential tunneling ionization ADK yield only (dashed line) and for the sum of the ADK ionization yield and NSI yield (solid line) due to the recollision ionization for C^{2+}, C^{3+}, and C^{4+} from the ionization of atomic carbon. As seen in Fig. 5, the measured C^+ and C^{2+} ion yields are consistently *lower* than the ADK yield near saturation by a factor of 20 and 2, respectively. For C^{3+} and C^{4+}, the measured yields are in good agreement with the calculated results near saturation. This implies that near saturation the C^+ and C^{2+} are produced through a nonatomic ionization process and the C^{3+} and C^{4+} are produced through atomic-like ADK ionization. Specifically, the result draws attention to the stabilizing effect hydrogen has in reducing the final state production of C^+ and C^{2+}. Hydrogen migration and dissociation from alkanes has been shown to be an important mechanism at 10^{14} W/cm^2 for slightly longer pulse durations (50 fs) [51]. The effect disappears at higher intensities when the hydrogen is fully ionized as is the case for C^{3+} and C^{4+}. This observation is consistent with the results from the fragmentation of alkanes by electron collision where hydrogen ions remove the charge from the ionized molecule. For example, as reported by [46], $CH_4^{2+} \rightarrow 2H^+ + CH_2$ is the dominant dissociation channel for

CH_4^{2+}. Below saturation (i.e., 1 ion/shot torr to 10^3 ions/shot torr) the measured C^+ ion yields remain lower than the ADK yield below saturation, but the yields of C^{2+}, C^{3+}, and C^{4+} are higher than the ADK yield.

For C^{2+} and C^{3+} the measured ion yields deviate only slightly from the atomic ADK yield below saturation. This slight deviation is consistent with the experimentally observed effect of the parent molecule ion size on the C^{2+} and C^{3+} yields (i.e., a molecular effect is present but it does not depend on the chain length size). One may begin to conclude at this point that C^+ is affected by nearest-neighbor hydrogen while C^{2+} and C^{3+} are affected by nearest-neighbor carbon and the stability of the fragments, which favors the production of $C_2H_n^+$ over other fragments. In the highest charge state measured C^{4+} we observe a clear and characteristic knee structure in the measured ion yield from 3.5×10^{14} to 4×10^{15} W/cm^2. Furthermore, the "knee" ionization in C^{4+} shows the greatest dependence on the molecular parent size. Continuing from the previous line of thought, it appears the C^{4+} ionization knee is sensitive to longer-range molecular structure, beyond just the nearest-neighbor carbons.

Our recollision model is able to predict just 1% of the NSI yield for C^{3+} and less than 1% for C^{2+} and C^{4+}. Since the C^{2+} through C^{4+} yields are dependent on the parent ion size below saturation, it is not unreasonable that the model is limited in its accuracy since it is based on atomic carbon. The authors note, however, at higher intensities with the C^{5+} fragments from methane, the model accurately predicts the sequential and nonsequential ionization yield observed experimentally [42]. The comparison with the experiment in Fig. 6 shows (1) the consistent suppression of the observed C^+ yield below that expected from the atomic model and (2) the excellent agreement near saturation for the production of C^{4+}.

A central issue in the ionization of polyatomic species, both clusters and molecules, is the dynamics for the electron and nuclear motion. In clusters the electron motion time scales are tunneling (~1 fs), "ignition" effects (~10 fs) [52], and resonant enhancement processes (~25 fs) [53]. The nuclear motion is primarily a Coulomb explosion and the hydrodynamic expansion which occur on 25 to 100 fs time scales [54]. In molecules, electron motion time scales include tunneling or photo-ionization (1 fs), rescattering (2 to 5 fs), and nonadiabatic multielectron dynamics [44] which can vary (10 to 100 fs). The actual charging of the molecule, that is, the time scale over which the electron leaves the molecular system after being ionized is on a similar time scale (~25 fs). Changes in the rescattering process have also been measured to vary on the 25 fs time scale according to pulse duration experiments on rescattering with atoms [55]. Nuclear dynamics in molecular systems can play a critical role in the absorption of energy from the laser such as with enhanced ionization at the critical bond distance [56]. The time scale for nuclear motion in enhanced ionization is typically 20 to 150 fs [57]. Coulomb explosion time scales vary but are similar to small clusters.

A simple free ion, Coulomb explosion calculation for the nuclear time scale in chain hydrocarbons is the time it takes the carbon bond to increase in length for a relevant species for the ultrahigh field like C^+-C^+. At a critical bond distance, R_c which is 2 to 3 times R_e the equilibrium bond distance [58], molecules typically undergo rapid ionization. For an initial R_c of 3.75 Å, two carbons C^+ and C^+ will take 10 fs to Coulomb explode to 1.5 R_c. To reach 3 R_c takes 20 fs or, in our experiments, roughly from the beginning of the pulse until the peak intensity. With higher charged species for comparison like C^+-C^{++} the dissociation time scale is 2 R_c in 10 fs. Experiments with Coulomb explosion imaging [14] have shown in strong fields the molecule bond angles and distance can change on a time scale of 25 fs for molecules comparable to the small hydrocarbons used here. Related studies with harmonics generated in organic molecules [59] demonstrated pulse duration effects when reducing the pulse from 240 to 70 fs and found many of the HHG features due to fragmentation and dissociation of the parent ion greatly reduced when the pulse duration was 70 fs. In these studies, the pulse duration is 35 fs (no difference is detected with the 45 fs pulses) and some of the related processes mentioned previously with 1 to 25 fs time scales are certainly involved in these studies (e.g., enhanced ionization, rescattering, Coulomb explosion). It is a reasonable approximation to assume the molecule is dissociating during the pulse duration and has time to reach R_c by the peak of the laser pulse. Geometric alignment effects [60] for the hydrocarbons are not expected to play a significant role in these studies based on the theoretical work in [61]. It is clear from these experiments that molecular structure does affect the ionization process even in the ultrastrong field. Previous to this study one may have presupposed the molecule is fully ionized in ultrastrong fields and the original molecular structure no longer affects the ionization process. Certainly follow up experiments with shorter or longer pulse durations will reveal new aspects to these dynamics in molecules and ultrastrong fields.

Finally, the rescattering mechanism has been invoked to explain the yields of doubly charged species in many molecular systems [62–65] including unsaturated alcohol chain hydrocarbons [66]. Based on recent work in methane [37] it is not clear that a simple extension of atomic rescattering applies to the fragments studied here. At this time the authors believe rescattering is a possible primary mechanism behind the yield for only C^{4+} and further studies with elliptically polarized light are underway to help determine the role of rescattering in the ionization of alkanes.

V. CONCLUSION

We have measured the molecular fragmentation and C^{n+} ($n \leqslant 4$) ion yields from ethane, butane, and octane at intensities from 4×10^{13} to 1×10^{17} W/cm^2 over eight orders of magnitude in signal. The molecular fragmentation studies show $C_2H_n^+$ are the highest yield fragments across the species and the fragmentation branching between different molecular ions does not exhibit a strong dependence on the laser intensity. The studies of C^{n+} fragments show C^+, and to a lesser extent C^{2+}, in a molecule is stabilized compared to ionization as a free atom. This is consistent with the results from electron collision ionization of alkanes where a dominant dissociation channel involves ionized hydrogen dissociating leaving a neutral C_nH_m fragment. The ADK results modeling the carbon as sequentially ionizing by tunneling from a free atom agree

with the measurements for C^{3+} and C^{4+} at saturation. Below saturation, the calculated NSI yields account for only about 1% of the C^{3+} ion yield and is less than 1% for the other carbon ions measured. When compared to the results from methane, larger molecules (ethane, butane, and octane) behave in a similar fashion, except the NSI yields increase as the molecule becomes larger. Lower charge states (C^{+}, C^{2+}, and C^{3+}) have a weak dependence on the parent molecular size while C^{4+} shows an order of magnitude change in the yield between methane and butane.

ACKNOWLEDGMENTS

This material is based upon work supported by the Army Research Office under Grant No. W911NF-09-1-0390 and the National Science Foundation under Grant No. 0757953.

[1] B. Friedrich and D. Herschbach, Phys. Rev. Lett. **74**, 4623 (1995).
[2] H. Stapelfeldt and T. Seideman, Rev. Mod. Phys. **75**, 543 (2003).
[3] C. Cornaggia, M. Schmidt, and D. Normand, J. Phys. B **27**, L123 (1994).
[4] M. J. J. Vrakking and S. Stolte, Chem. Phys. Lett. **271**, 209 (1997).
[5] J. J. Larsen, K. Hald, N. Bjerre, H. Stapelfeldt, and T. Seideman, Phys. Rev. Lett. **85**, 2470 (2000).
[6] F. Rosca-Pruna and M. J. J. Vrakking, J. Chem. Phys. **116**, 6567 (2002).
[7] E. E. Aubanel, J. M. Gauthier, and A. D. Bandrauk, Phys. Rev. A **48**, 2145 (1993).
[8] K. Codling, L. J. Fransinski, and P. A. Hatherly, J. Phys. B **22**, L321 (1995).
[9] C. Guo, R. T. Jones, and G. N. Gibson, Phys. Rev. A **62**, 015402 (2000).
[10] A. Jaron-Becker, A. Becker, and F. H. M. Faisal, Phys. Rev. A **69**, 023410 (2004).
[11] M. Ivanov, T. Seideman, P. Corkum, F. Ilkov, and P. Dietrich, Phys. Rev. A **54**, 1541 (1996).
[12] P. Hering and C. Cornaggia, Phys. Rev. A **59**, 2836 (1999).
[13] K. Zhao and W. T. Hill, Phys. Rev. A **71**, 013412 (2005).
[14] F. Legare, K. F. Lee, I. V. Litvinyuk, P. W. Dooley, A. D. Bandrauk, D. M. Villeneuve, and P. B. Corkum, Phys. Rev. A **72**, 052717 (2005).
[15] P. Hering and C. Cornaggia, Phys. Rev. A **57**, 4572 (1998).
[16] S. M. Hankin, D. M. Villeneuve, P. B. Corkum, and D. M. Rayner, Phys. Rev. Lett. **84**, 5082 (2000).
[17] A. Jaron-Becker, A. Becker, and F. H. M. Faisal, Phys. Rev. A **69**, 023410 (2004).
[18] S. Shimizu, J. Kou, S. Kawato, K. Shimizu, S. Sakabe, and N. Nakshima, Chem. Phys. Lett. **317**, 609 (2000).
[19] X. M. Tong, Z. X. Zhao, and C. D. Lin, Phys. Rev. A **66**, 033402 (2002).
[20] M. V. Ammosov, N. B. Delone, and V. P. Krainov, Sov. Phys. JETP **64**, 1191 (1986).
[21] M. Tanaka, M. Murakami, T. Yatsuhashi, and N. Nakashima, J. Chem. Phys. **127**, 104314 (2007).
[22] D. Mathur, T. Hatamoto, M. Okunishi, G. Prümper, T. Lischke, K. Shimada, and K. Ueda, J. Phys. Chem. A **111**, 9299 (2007).
[23] C. Y. Wu, Z. Wu, Q. Liang, M. Liu, Y. Deng, and Q. Gong, Phys. Rev. A **75**, 043408 (2007).
[24] Z. F. Wu, C. Y. Wu, Q. Q. Liang, S. Wang, M. Liu, Y. Deng, and Q. Gong, J. Chem. Phys. **126**, 074311 (2007).
[25] C. Y. Wu, H. Z. Ren, T. T. Liu, R. Ma, H. Yang, H. B. Jiang, and Q. H. Gong, J. Phys. B **35**, 2575 (2002).
[26] A. N. Markevitch, D. A. Romanov, S. M. Smith, H. B. Schlegel, M. Y. Ivanov, and R. J. Levis, Phys. Rev. A **69**, 013401 (2004).
[27] P. B. Corkum, M. Y. Ivanov, and J. S. Wright, Annu. Rev. Phys. Chem. **48**, 387 (1997).
[28] J. H. Posthumus, A. J. Giles, M. R. Thompson, and K. Codling, J. Phys. B **29**, 5811 (1996).
[29] K. Codling and L. J. Frasinski, J. Phys. B **26**, 783 (1993).
[30] S. Micheau, Z. Chen, A. T. Le, and C. D. Lin, Phys. Rev. A **79**, 013417 (2009).
[31] A. L'Huillier and P. Balcou, Phys. Rev. Lett. **70**, 774 (1993).
[32] H. Niikura, F. Legare, R. Hasbani, M. Yu. Ivanov, D. M. Villeneuve, and P. B. Corkum, Nature (London) **421**, 826 (2003).
[33] S. Baker, J. S. Robinson, C. A. Haworth, H. Teng, R. A. Smith, C. C. Chirila, M. Lein, J. W. G. Tisch, and J. P. Marangos, Science **312**, 424 (2006).
[34] M. Hohenberger, D. R. Symes, K. W. Madison, A. Sumeruk, G. Dyer, A. Edens, W. Grigsby, G. Hays, M. Teichmann, and T. Ditmire, Phys. Rev. Lett. **95**, 195003 (2005).
[35] J. Zweiback, T. E. Cowan, J. H. Hartley, R. Howell, K. B. Wharton, J. K. Crane, V. P. Yanovsky, G. Hays, R. A. Smith, and T. Ditmire, Phys. Plasmas **9**, 3108 (2002).
[36] I. Last and J. Jortner, J. Phys. Chem. A **106**, 10877 (2002).
[37] S. Palaniyappan, R. Mitchell, R. Sauer, I. Ghebregziabher, S. L. White, M. F. Decamp, and B. C. Walker, Phys. Rev. Lett. **100**, 183001 (2008).
[38] J. Z. H. Yang and B. C. Walker, Opt. Lett. **26**, 453 (2001).
[39] A. D. DiChiara *et al.*, Opt. Lett. **28**, 2106 (2003).
[40] J. Ullrich, R. Moshammer, A. Dorn, R. Dorner, L. P. H. Schmidt, and H. Schniidt-Bocking, Rep. Prog. Phys. **66**, 1463 (2003).
[41] T. Weber, H. Giessen, M. Weckenbrock, G. Urbasch, A. Staudte, L. Spielberger, O. Jagutzki, V. Mergel, M. Vollmar, and R. Dorner, Nature (London) **405**, 658 (2000).
[42] S. Palaniyappan *et al.*, J. Phys. B **39**, S357 (2006).
[43] T. Cechan and C. R. Vidal, Chem. Phys. Lett. **288**, 499 (1998).
[44] M. Lezius, V. Blanchet, M. Y. Ivanov, and A. Stolow, J. Chem. Phys. **117**, 1575 (2002).
[45] F. N. Kong, Q. Luo, H. L. Xu, M. Sharifi, D. Song, and S. L. Chin, J. Chem. Phys. **125**, 133320 (2006).
[46] P. Q. Wang and C. R. Vidal, Chem. Phys. **280**, 309 (2002).
[47] D. Zeidler, A. Staudte, A. B. Bardon, D. M. Villeneuve, R. Dorner, and P. B. Corkum, Phys. Rev. Lett. **95**, 203003 (2005).
[48] B. Walker, B. Sheehy, L. F. DiMauro, P. Agostini, K. J. Schafer, and K. C. Kulander, Phys. Rev. Lett. **73**, 1227 (1994).
[49] NIFS DATABASE at [https://dbshino.nifs.ac.jp].
[50] K. Gluch *et al.*, Int. J. Mass Spectrom. **228**, 307 (2003).

[51] K. Hoshina, Y. Furukawa, T. Okino, and K. Yamanouchi, J. Chem. Phys. **129**, 104302 (2008).
[52] C. Rose Petruck, K. J. Schafer, K. R. Wilson, and C. P. J. Barty, Phys. Rev. A **55**, 1182 (1997).
[53] I. Last and J. Jortner, Phys. Rev. A **60**, 2215 (1999).
[54] T. Ditmire, E. Springate, J. W. G. Tisch, Y. L. Shao, M. B. Mason, N. Hay, J. P. Marangos, and M. H. R. Hutchinson, Phys. Rev. A **57**, 369 (1998).
[55] V. R. Bhardwaj, S. A. Aseyev, M. Mehendale, G. L. Yudin, D. M. Villeneuve, D. M. Rayner, M. Y. Ivanov, and P. B. Corkum, Phys. Rev. Lett. **86**, 3522 (2001).
[56] S. Menon, J. P. Nibarger, and G. N. Gibson, J Phys. B **35**, 2961 (2002).
[57] S. Chelkowski and A. D. Bandrauk, J. Phys. B **28**, L723 (1995).
[58] K. Zhao, G. Zhang, and W. T. Hill, Phys. Rev. A **68**, 063408 (2003).
[59] N. Hay, R. de Nalda, T. Halfmann, K. J. Mendham, M. B. Mason, M. Castillejo, and J. P. Marangos, Phys. Rev. A **62**, 041803 (2000).
[60] S. Banerjee, G. R. Kumar, and D. Mathur, Phys. Rev. A **60**, R3369 (1999).
[61] A. Jaron-Becker, A. Becker, and F. H. M. Faisal, Phys. Rev. A **69**, 023410 (2004).
[62] A. I. Pegarkov, E. Charron, and A. Suzor-Weiner, J. Phys. B **32**, L363 (1999).
[63] A. Talebpour, S. Larochelle, and S. L. Chin, J. Phys. B **30**, L245 (1997).
[64] C. Cornaggia and Ph. Hering, J. Phys. B **31**, L503 (1999).
[65] S. Menon, J. P. Nibarger, and G. N. Gibson, J. Phys. B **35**, 2961 (2002).
[66] F. A. Rajgara, M. Krishnamurthy, and D. Mathur, J. Chem. Phys. **119**, 12224 (2003).